energies

MDPI

Article

Hydrogen Photo-Production from Glycerol Using Nickel-Doped TiO$_2$ Catalysts: Effect of Catalyst Pre-Treatment

Jesús Hidalgo-Carrillo *[ID]**, Juan Martín-Gómez, Julia Morales, Juan Carlos Espejo, Francisco José Urbano**[ID] **and Alberto Marinas**[ID]

Departamento de Química Orgánica, Instituto Universitario de Investigación en Química Finay Nanoquímica (IUNAN), Universidad de Córdoba, E-14071 Córdoba, Spain

* Correspondence: jesus.hidalgo@uco.es

check for updates

Abstract: In the present piece of research, hydrogen production via the photo-reforming of glycerol (a byproduct from biodiesel generation) is studied. Catalysts consisted of titania modified by Ni (0.5% by weight) obtained through deposition–precipitation or impregnation synthetic methods (labelled as Ni-0.5-DP and Ni-0.5-IMP, respectively). Reactions were performed both under UV and solar irradiation. Activity significantly improved in the presence of Ni, especially under solar irradiation. Moreover, pre-reduced solids exhibited higher catalytic activities than untreated solids, despite the "in-situ" reduction of nickel species and the elimination of surface chlorides under reaction conditions (as evidenced by XPS). It is possible that the catalyst pretreatment at 400 °C under hydrogen resulted in some strong metal–support interactions. In summary, the highest hydrogen production value (ca. 2600 micromole H$_2$·g^{-1}) was achieved with pre-reduced Ni-0.5-DP solid using UV light for an irradiation time of 6 h. This value represents a 15.7-fold increase as compared to Evonik P25.

Keywords: hydrogen production; photo-reforming; glycerol; Ni/TiO$_2$

1. Introduction

Fossil fuel depletion and environmental concerns have resulted in the search for clean energies, with one alternative being hydrogen [1]. Its use has two main advantages [2,3]: i) a high chemical energy per mass (120 KJ/g), superior to that of many fossil fuels, and ii) its combustion only results in water; therefore, it does not emit any toxic substance or greenhouse gas into the atmosphere.

Nevertheless, hydrogen does not exist in nature in its molecular H$_2$ form but combined to other elements; thus, it requires dedicated methods for its production. Therefore, whether or not the use of hydrogen as an energy vector can be termed as "fully green" is dependent on its method of production.

Currently, the most widespread hydrogen production methodologies are hydrocarbon reforming with water vapor and water electrolysis. Hydrocarbon reforming has the disadvantages of being based on raw materials which are taken from non-renewable fossil sources and, therefore, the co-generated CO$_2$ directly impacts the environment by the greenhouse effect. An additional drawback of hydrocarbon reforming with water vapor is its high operating temperature. On the other hand, regarding the production of hydrogen through water electrolysis, its main associated problem is the high consumption of electrical energy to carry out the process. Solar thermal energy can be used as an alternative for water electrolysis but, in this case, large and expensive facilities are needed.

Recently, in addition to the mentioned technologies, innovative techniques have been being developed and could be complementary to those already existing in the medium-term future. Some of these hydrogen production techniques are plasma technology [4], biological production methods such

as dark fermentation [5,6] or the photocatalytic reforming of oxygenated organic compounds [7,8]. The photocatalytic reforming of oxygenated organic compounds consists in the treatment of these compounds with light radiation in the presence of water, at room temperature and under anaerobic conditions, to generate gaseous hydrogen and carbon dioxide. The potential of hydrogen production through photocatalytic reforming is fulfilled when biomass residues (bio-glycerol or glucose, among others) are used as oxygenated organic compounds since, in this case, the generated CO_2 was previously consumed by the biomass during its growth, so there is no net emission of CO_2 but a closing of the carbon cycle [9]. In the process, light is used to activate a semiconductor, promoting electrons from the valence to the conduction band. The oxygenated organic compound is used as a sacrificial agent to favor the elimination of the positively-charged holes, whereas electrons are used to reduce protons and generate H_2. As for the sacrificial agents, glycerol is an excellent candidate since it is a by-product of biodiesel production [10].

One of the keys to the success of this emergent technology is the development of suitable catalysts (i.e., semiconductors) which are able to maximize light harvesting and therefore the hydrogen production [11]. TiO_2 is the most widely used semiconductor as a result of its high photocatalytic activity and due to the fact that it is inexpensive, not toxic and biologically and chemically inert [12]. Its main drawback is its band gap value (ca. 3.2 eV), which means that only ca. 5% of solar irradiation is absorbed. Furthermore, it also exhibits a high electron–hole recombination rate, which is detrimental to the photocatalytic activity [13].

One alternative to overcome these problems is the incorporation of metals to the semiconductor [14] (Figure 1), which can shift the absorption to the visible light and also act as electron traps, thus preventing electron–hole recombination. Noble metals such as silver [15], gold [16], platinum [17] or palladium [18] have been found to be particularly effective, although there is a need to implement some more cost-effective transition metals such as iron [19], nickel [20,21] and copper [22,23].
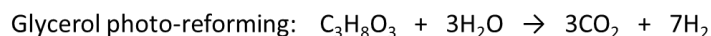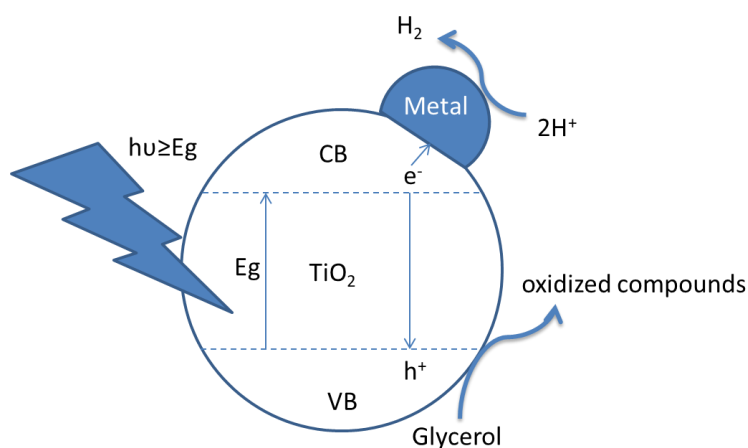

Glycerol photo-reforming:　$C_3H_8O_3$　+　$3H_2O$　→　$3CO_2$　+　$7H_2$

Figure 1. Activation of titania using a metal as a co-catalyst.

In the present piece of research, nickel structural (particle size) and chemical properties (oxidation state) in Ni-modified titania photocatalysts has been addressed, and their influence on hydrogen production from glycerol photo-reforming studied. Two catalyst synthetic methods (impregnation vs. deposition–precipitation) and catalyst pre-reduction treatment were analyzed and their influence on the amount of hydrogen photo-produced revealed under both UV and solar radiation.

2. Materials and Methods

2.1. Catalysts Synthesis

2.1.1. Deposition–precipitation Method

The deposition-precipiation method was used for incorporation of nickel on P25 Evonik with a nominal weight of 0.5%. The incorporation of Nickel was carried out in a "Contalab" system (Switzerland) enabling careful control of all the variables, i.e., pH, temperature, stirrer speed, reactant feed flow, etc. Firstly in 150 mL distilled water were dispersed 5 g of P25 Evonik using ultrasound. The deposition of the nickel was carried out at 60 °C and a pH of 6.8, keeping it constant with an 0.2 M aqueous solution of K_2CO_3 (Sigma Aldrich). Next, an aqueous solution of 2 g·L^{-1} of nickel (using $NiCl_2$ (Sigma Aldrich)) was added dropwise and the mixture was maintained for 1 h at 60 °C. Then the solid obtained was filtered and washed with distilled water. Then, the solid was dried at 110 °C overnight. Finally, the solids were calcined at 400 °C for 6 h (using a ramp rate of 10 °C·min^{-1}).

2.1.2. Impregnation Method

A total of 5 g of TiO_2 (P25 Evonik) was dispersed in 100 mL of distilled water containing the required amount of $NiCl_2$ (Sigma Aldrich) aqueous solution in order to have a nickel nominal content of 0.5% by weight. The suspension was stirred for 1 h and then vacuum filtered at 100 °C. Then, the solid was dried overnight (100 °C) and calcined at 400 °C for 6 h (ramp rate 10 °C·min^{-1}).

The catalyst nomenclature includes the metal (Ni), the nominal content (0.5% by weight) and a suffix indicating the synthetic method (DP or IMP for deposition–precipitation or impregnation, respectively).

2.1.3. Catalyst Pre-Reduction

The catalysts were used either as synthesized or after a pre-reduction treatment. In the latter case, the solids were treated at room temperature under N_2 flow (20 mL·min^{-1}) for 15 min and then submitted to hydrogen (10mL·min^{-1}), the temperature being ramped up to 400 °C (rate, 10 °C·min^{-1}) and the final temperature being maintained for 1 h. The nomenclature of pre-reduced solids includes the "Red" suffix.

2.2. Characterization of the Solids

The determination of the metallic content in the samples was carried out by by inductively coupled plasma mass spectrometry (ICP-MS) using a Perkin Elmer NexionX instrument. Digestion of the samples consisted in dissolution of the sample in an acid solution of 1:1 $H_2O/H_2SO_4/HF$ solution at 80 °C and and after in 1:3 HNO_3/HCl mixture. The measurements were carried out by the staff at the Central Service for Research Support (SCAI) of the University of Córdoba.

Transmission electron microscopy (TEM) images were obtained with a JEOL JEM 1400 transmission electron microscope. For the measurements were used a 3 mm holey carbon copper grids. Particle sizes were obtained using using the software ImageJ (a public domain Java image processing and analysis program). TEM was carried out at the Central Service for Research Support (SCAI) of the University of Córdoba.

X-ray diffraction (XRD) analysis was performed on a D8 Discover instrument (Bruker Corporation, Billerica, USA) using CuKα radiation over the range 5–80°.

A Cary 1E (Varian) instrument was used for determination of Band Gap values by Diffuse reflectance UV–vis spectra, using as reference material the polytetraethylene (density = 1 g·cm^{-3} and thickness = 6 mm). The plot of the modified Kubelka–Munk function $[F(R)·E]^{1/2}$ versus the energy of the absorbed light E was use to obtain the value of band gap, extrapolating to y = 0 of the linear regression range.

X-ray photoelectron spectroscopy (XPS) data were recorded by a Leibold–Heraeus LHS10 spectrometer capable of operating down to less than 2×10^{-9} Torr, was equipped with an EA-200MCD hemispherical electron analyzer with a dual X-ray source using AlKα(hv = 1486.6 eV) at 120 W, at 30 mA, with C (1s) as energy reference (284.6 eV). The sample was prepared in a on 4 mm $\times$ 4 mm pellets 0.5 mm thick, and outgassing to a pressure below about 2×10^{-8} Torr at 150 °C in the instrument pre-chamber. XPS experiments were carried out at the Central Service for Research Support (SCAI) of the University of Córdoba.

In an Autochem 2920 analyser (Micromeritics Instrument Corp., Norcross, GA, USA) was carried out the Temperature-programmed reduction (TPR) measurements, 200 mg of the solids was used to carried out the experiment with a flow of 40 mL·min^{-1} of a 5% H_2/Ar stream. The temperature was ramped from room temperature to 500 °C at 10 °C·min^{-1}.

2.3. Photocatalytic Experiments

Photocatalytic experiments were performed in a 30 mL double -mouthed heart-shaped reactor under UV light irradiation (UV Spotlight source Lightningcure^{TM} L8022, Hamamatsu, maximum emission at 365 nm) or solar irradiation (Newport, Xe lamp). Light was focalized on the sample compartment through an optic fiber. In a typical process, 5 mg of catalyst was dispersed into 5 mL of glycerol/water (10% *v/v*) solution. Reactions were performed under an inert atmosphere, achieved by bubbling a nitrogen flow (20 mL·min^{-1}) for 30 min. The catalyst suspension was continuously stirred (800 rpm) and the reactor was thermostated at 20 °C. A picture of the photocatalytic reactor is shown in Figure 2.
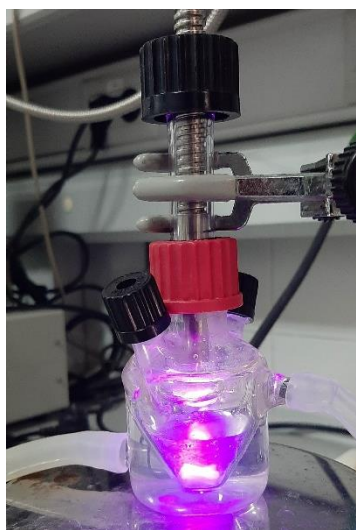

Figure 2. Picture of the photocatalytic reactor used in the hydrogen production from glycerol photo-reforming.

Hydrogen was analyzed by sampling with a pressure-lock precision analytical syringe (Valco VICI Precision Syringes, 1 mL, leak-tight to 250 psi) from the head space after 3 and 6 h of irradiation. Analyses were performed on an Agilent Technologies 7890A gas chromatograph equipped with a Supelco Carboxen^{TM} 1010 Plot column with TCD detector. The separation was performed at 70 °C for 2 min, followed by heating to 120 °C (ramp of 10 °C·min^{-1}), and was left for 8 min (total analysis time, 15 min). All reactions were performed in duplicate, with the standard deviation being below 3%. The calibration plot (Figure S1) and a typical chromatogram for hydrogen quantification (Figure S2) are given in the Supplementary Materials.

3. Results and Discussion

The synthesized catalysts were characterized from the structural and chemical point of view with a wide variety of techniques. The chemical composition was determined by ICP-MS and the results, presented in Table 1, evidenced a good incorporation of nickel, with values being quite close to the nominal content (0.5% by weight).

Table 1. Metallic content of the solids as determined by inductively-coupled plasma mass spectrometry (ICP-MS). DP: deposition–precipitation; IMP: impregnation.

Catalyst	Ni Nominal Content (weight%)	Experimental Ni Content (ICP-MS, weight%)
Ni-0.5-DP	0.50	0.55
Ni-0.5-IMP	0.50	0.47

X-ray diffraction patterns were obtained and used to obtain structural information of the catalysts, and the results are presented in Figure S3. The Evonik P25 support clearly shows the diffraction lines corresponding to anatase (80%) and rutile (20%) phases, which are not affected by nickel incorporation, independent of the synthetic method or reduction treatment. In addition, consistent with the small metal loading and the homogeneous nickel dispersion evidenced by TEM micrographs, no signals associated to nickel species are observed.

Temperature-programmed reduction (TPR) measurements were carried out for both Ni-0.5-DP and Ni-0.5-IMP catalysts, and the results are presented in Figure 3 (right). These results showed that the reduction peaks associated with nickel species begin at temperatures below 200 °C but extend to 400 °C.
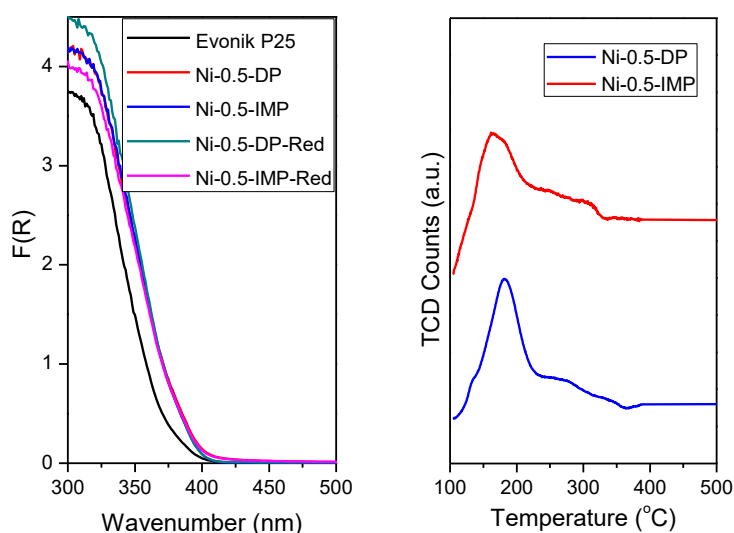

Figure 3. UV-vis spectra (**left**) and temperature-programmed reduction profiles (**right**) obtained for the catalysts prepared in this work.

It is well known that NiO is usually the main surface species when nickel is deposited in high loads on metal oxide-type supports. However, certain species from the Ni–support interaction can be observed depending on the physicochemical properties of the support. It has been reported that the reduction of certain nickel species is difficult in supported nickel catalysts, with this difficulty being proportional to the strength of the Ni–support interaction [24]. In general, the Ni–support interaction falls into three categories: i) an absence of interaction, which occurs when the support acts as a mere dispersing agent, ii) a weak interaction, usually associated with the presence of small nickel nanoparticles deposited on the support; and iii) a very strong interaction, involving the formation of a

new surface species (creation of new chemical bonds). The degree of interaction depends on the nickel charge (particle size) and the calcination temperature of the catalyst [24].

It has been reported that the reduction of unsupported NiO takes place at temperatures of around 220 °C [24], while the presence of metal–support interactions extend the nickel reduction process to higher temperatures. However, Petrik et al. associated the observed reduction peak at 200 °C to the reduction of Ni_2O_3 (ions with formal oxidation state higher than +2) to NiO [25]. In this sense, Carley et al. demonstrated, through XPS studies, the massive formation of surface Ni^{3+} species after the calcination of the solid at temperatures above 300 °C [26]. Finally, the reduction peaks observed at higher temperatures (300–600 °C) were associated with the reduction of the previously formed NiO species or to the reduction of small nanoparticles interacting with the TiO_2 support [25].

Based on the above considerations, the observed reduction peak at about 200 °C could be associated with either the reduction of bulk NiO or with the reduction of Ni^{+3} species (nickel ions with a formal oxidation state higher than +2) [25,26]. Given the low nickel loading (0.5%) as well as the small particle sizes reported by TEM (2 and 4 nm for Ni-0.5-DP and Ni-0.5-IMP, respectively), it is more feasible to associate the reduction peak at 200 °C with the reduction of Ni^{+3} species present in the catalyst. Reduction peaks observed at higher temperatures would be associated with small NiO particles interacting with the titania support. According to these results, the temperature chosen for catalyst reduction was set to 400 °C.

Band-gap energy values of the semiconductors were determined from UV-Vis spectra. The method for the determination of band gap values is shown in Figure S4 using the example of Ni-0.5-IMP-Red. As can be seen, the modification of the reference titania material (Evonik P25) by nickel incorporation resulted in a slight decrease in the band gap (Table 2), with the absorption being shifted to the visible spectrum (Figure 3, left)

Table 2. Band-gap energy values of the solids as determined by UV-Vis spectroscopy.

Catalyst	Eg (eV)	Catalyst	Eg (eV)
P25	3.11		
Ni-0.5-DP	3.02	Ni-0.5-DP-Red	3.07
Ni-0.5-IMP	3.00	Ni-0.5-IMP-Red	3.01

TEM micrographs of the different solids are shown in Figures 4–6, and the particle size distribution is shown in Figure S5. Ni particle sizes were determined using ImageJ software. The deposition–precipitation method resulted in particles with an average size of 2 nm, whereas the impregnation method led to more heterogeneously-distributed sizes (Figure S5), with the average particle size being 4–5 nm. Particle sizes did not vary significantly after the pre-reduction treatment.

Furthermore, the Ni particle size did not vary significantly after the first use. In the case of the utilization of UV light, there were no changes either after the second use. On the contrary, when solar irradiation was applied, the Ni particle size in the Ni-0.5-DP sample increased up to 5 nm (Figure 6).

The surface chemical composition of the solids was studied by XPS, and the main results are summarized in Table 3. As far as the Ti (2p3/2) signal is concerned, there were no significant changes after the incorporation of nickel, with the signal appearing at ca. 458.5 eV, which is a typical value for Ti^{4+} in TiO_2. Regarding the Ni 2p3/2 signal, it has been reported that binding energies at 852.6, 854.6, and 856.1 eV correspond to Ni^0, Ni^{+2}, and Ni^{+3}, respectively [25,27]. As we have commented previously, based on XPS data, Carley et al. unequivocally demonstrated the existence of Ni^{+3} species in nanostructured solids calcined at temperatures above 300 °C [26].
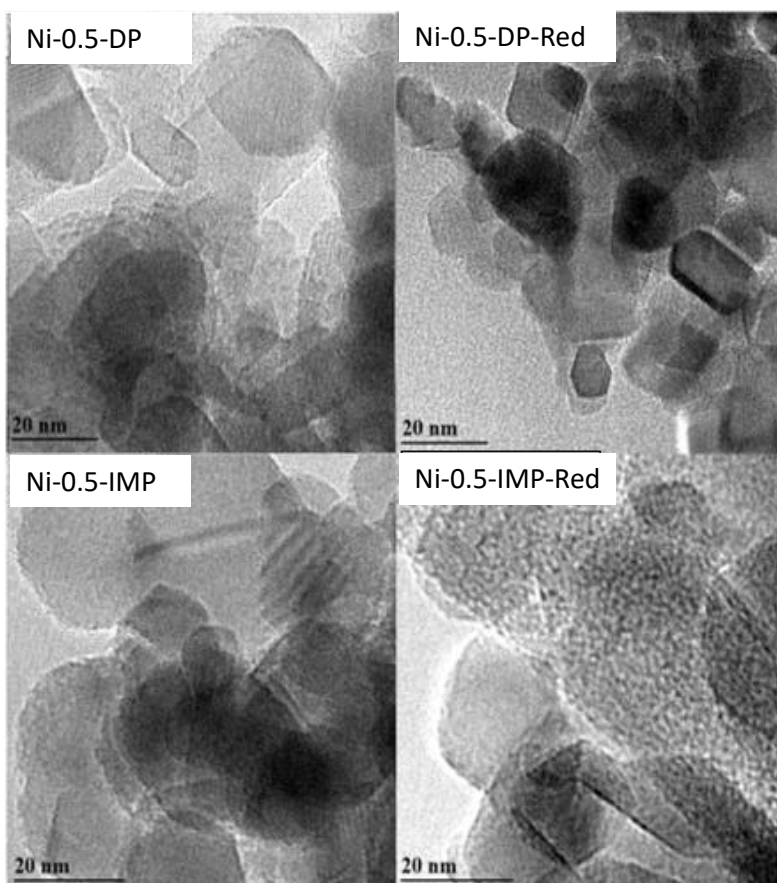
Figure 4. TEM micrographs of the fresh (unused) Ni catalysts.

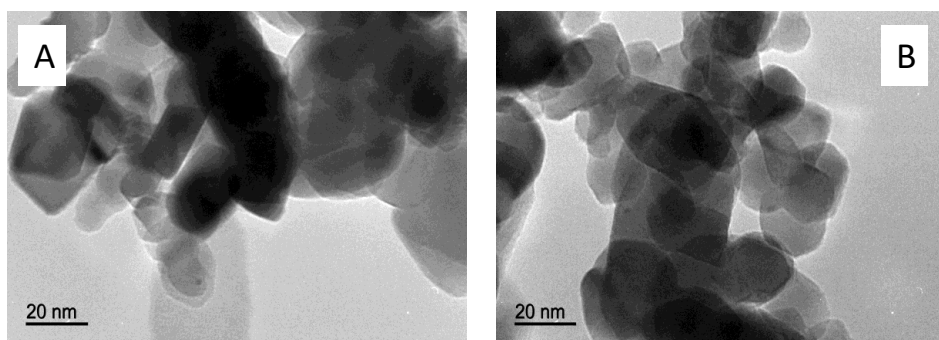**Figure 5.** TEM micrographs of Ni-0.5-DP solid after the reaction under UV (**A**) or solar (**B**) irradiation.
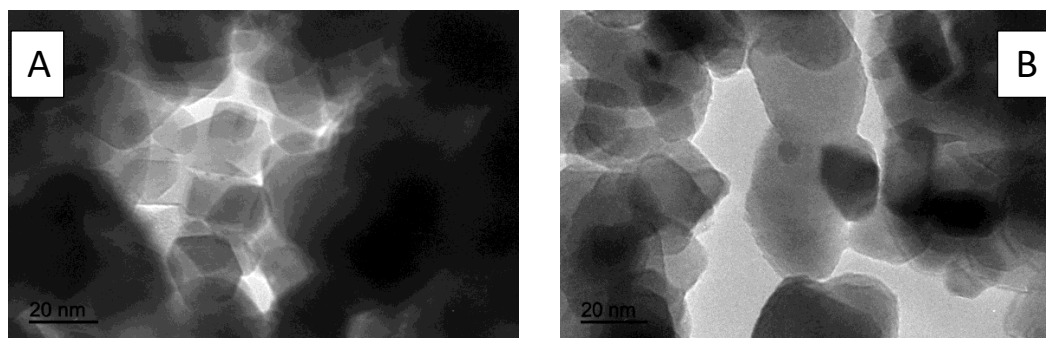

Figure 6. TEM micrographs of Ni-0.5-DP solid after the second reutilization using UV (**A**) or solar (**B**) irradiation.

Table 3. Ni (2p3/2), Ti (2p3/2) and Cl (2p) binding energies (eV) as determined by XPS.

Catalyst	Ni (2p3/2)	Ti (2p3/2)	Cl (2p)
Ni-0.5-DP	855.9	458.8	199.9
Ni-0.5-DP-Red	855.0	458.7	-
Ni-0.5-IMP	856.1	458.8	200.0
Ni-0.5-IMP-Red	855.1	458.5	-
Ni-0.5-DP 1 using UV	854.9	458.6	-
Ni-0.5-DP 1 using solar	855.1	458.6	-
Ni-0.5-DP 2 using UV	855.2	458.4	-
Ni-0.5-DP 2 using solar	854.9	458.4	-

Moreover, Petrik et al., working with nanosized nickel oxides, found that binding energies at 855.3 and 856.7 eV were typical for Ni/TiO_2 systems, with the signal at around 856 eV being preferably associated with Ni_2O_3 rather than with NiO, whose signal appeared at around 855 eV. The authors thus speculated the existence of Ti–Ni–O interactions that were reflected as Ni^{+3} species in the XPS spectra [25].

In this work, the XPS data associated with Ni (2p3/2) signals are presented in Table 3 and Figure S6. The spectra showed a signal at ca. 856 eV for fresh unreduced solids which was assigned to Ni^{+3} species, whereas, after the reduction treatment, the signal shifts to 855 eV as a result of the reduction of Ni^{+3} to Ni^{+2} species. This is in agreement with the reduction peak observed in the TPR profile at around 200 °C. Moreover, in the XPS analysis of the non-reduced catalysts used in a photo-reforming process (both UV and solar), the Ni (2p3/2) signal appears at ca. 855 eV, indicating that during the photocatalytic process, the in-situ reduction of Ni^{+3} to Ni^{+2} species takes place (Figure S6). No signal associated to Ni metal was detected in XPS profiles, even for the reduced solids, and so the catalyst reduction at 400 °C would not be strong enough to carry out the NiO reduction to Ni^0, or else the hypothetically formed Ni^0 would re-oxidize in contact with air. In this sense, Ju et al. have already reported the absence of the Ni (0) peak at 852 eV after the reductive treatment of nickel-containing absorbents, were was associated with the difficulty of reducing NiO to metallic nickel [28].

It is also interesting to note that XPS revealed the presence of chlorine from the precursor in fresh unreduced solids (0.56 and 0.80 atomic % for Ni-0.5-IMP and Ni-0.5-DP, respectively). Such chlorine atoms were eliminated either during pre-reduction treatment as HCl or during the photocatalytic reaction.

H_2 production from glycerol photo-reforming on fresh unreduced catalysts after 3 and 6 h of UV (A) or solar (B) irradiation are given in Figure 7. For the sake of comparison, results obtained for the reference material (Evonik P25) have also been included.

A first conclusion from Figure 7 is that hydrogen production using UV light is always higher than that achieved with solar light. This is hardly surprising, considering that the former irradiation source is more energetic. Moreover, Ni incorporation to TiO_2 (irrespective of the method) led to an increase in hydrogen production. For instance, when UV light was used, hydrogen production increased from 166 micromole·g^{-1} (Evonik P25) up to 534 (Ni-0.5-DP) or 551 (Ni-0.5-IMP) after $t = 6$ h. Such an increase is even more significant when visible light was used. The observed shift of UV-Vis absorption to the visible region on the introduction of Ni could account for this effect.

A comparison of hydrogen production on pre-reduced (Figure 8) and untreated systems (Figure 7) allows us to conclude that catalyst pre-reduction treatment significantly increases catalytic activity (3–5 fold or 8–9 fold for experiments under UV or solar irradiation, respectively). As with the untreated systems, there are no large differences in their catalytic behavior depending on the synthesis procedure (DP or IMP). In the pre-reduced systems, those synthesized by DP have 39% greater activity, which could be due to the more homogeneous particle size distribution of Ni.
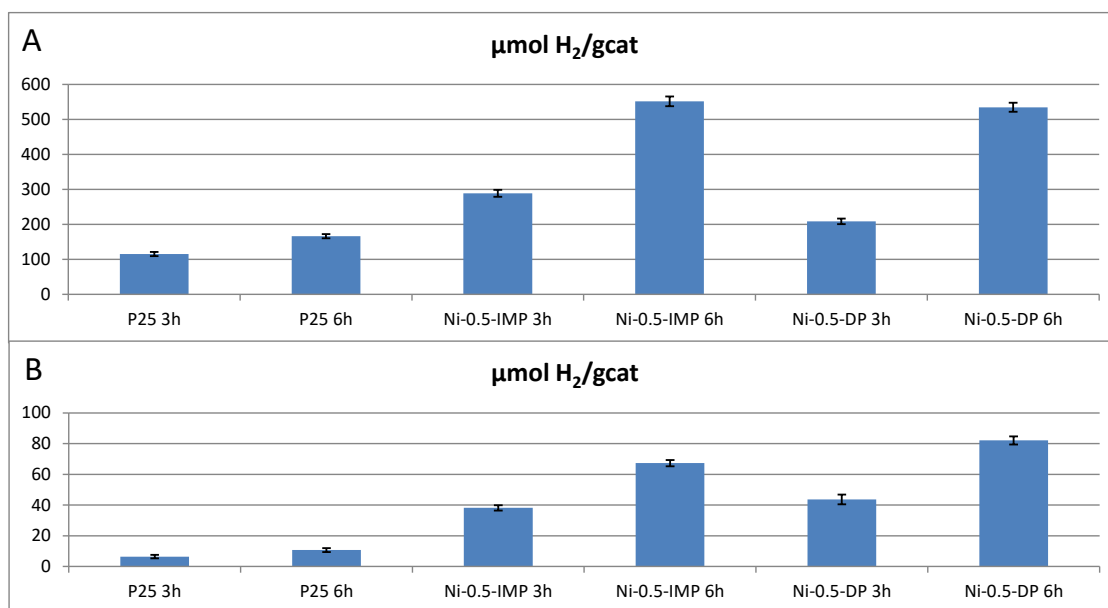
Figure 7. H_2 production from glycerol photo-reforming on fresh, unreduced solids using UV (**A**) and solar (**B**) irradiation.
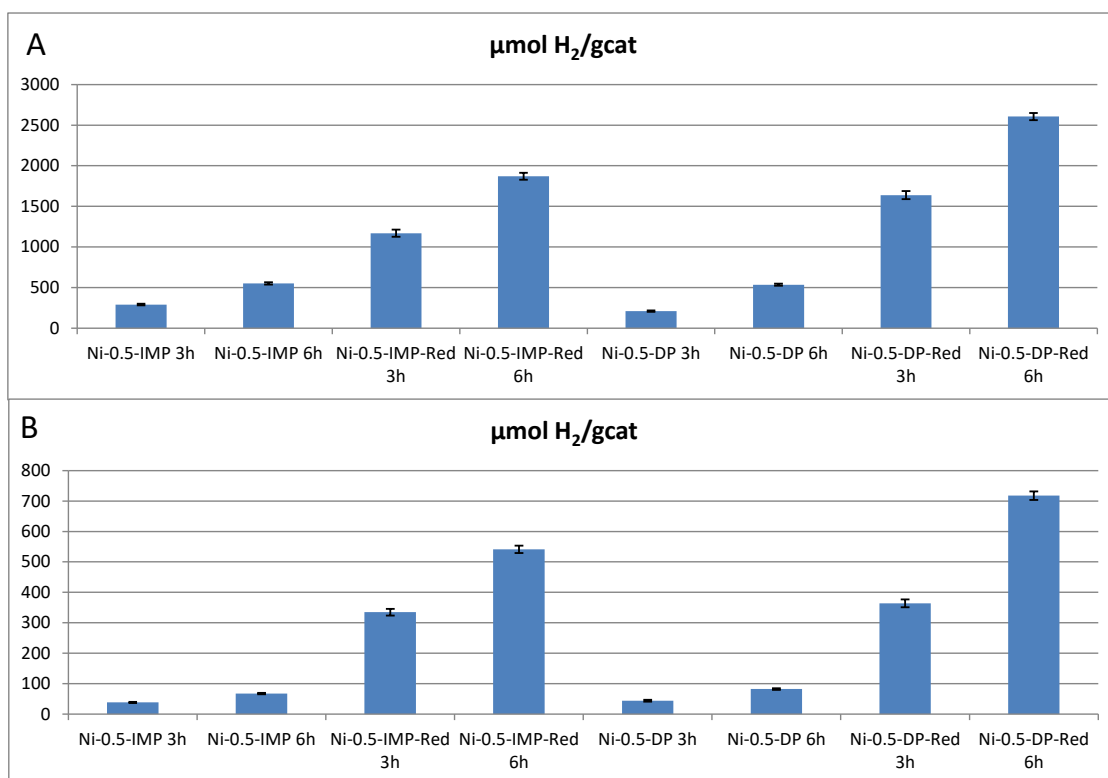

Figure 8. H_2 production via glycerol photo-reforming on untreated and pre-reduced solids using UV (**A**) and solar (**B**) irradiation.

The highest hydrogen production values (2606 H_2 micromole·g^{-1}) corresponded to Ni-0.5-DP-Red for $t = 6$ h. This value is similar to that achieved in previous studies on 0.2% Pt [29], which is quite promising considering that Pt is ca. 2000 times more expensive than Ni.

Some authors, such as Bahruji et al. [30], have described the influence of the metal oxidation state on the photocatalytic process. As can be seen in Figure 9B, the electron transfer from titania to NiO is thermodinamically impeded. On the contrary, the pre-reduction of the solid (Figure 9A) results in

electron transfer from titania to Ni(0) being favored, with the metal thus acting as an electron trap and preventing electron–hole recombination.
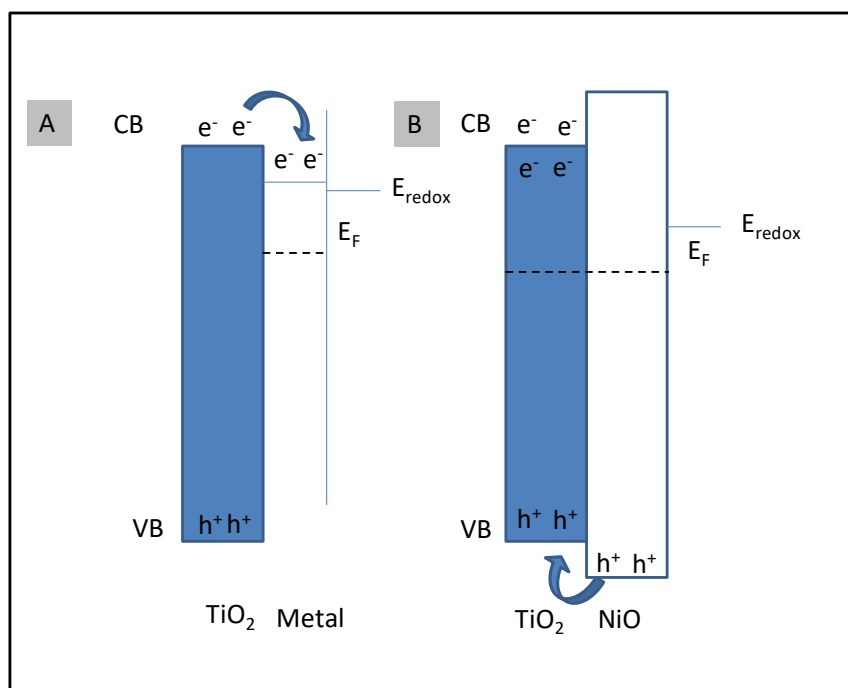

Figure 9. Energy levels of (**A**) TiO$_2$/metal and (**B**) TiO$_2$/NiO, adapted from Bahruji et al [30].

Furthermore, Caravaca et al. [31], studying hydrogen photo-production from sugars on Ni-based catalysts, observed an induction period (in their case, 60 min) required for in-situ reduction of NiO to Ni. After that period of time, the hydrogen production rate of both the untreated and pre-reduced solid was the same. According to these reports, we asume the in-situ reduction of our catalysts during reactions, and so the electron transfer from titania to Ni(0) is favored [30].

Another possible explanation for the observed better catalytic performance of pre-reduced solids as compared to untreated systems is the presence in the latter solids of surface chlorides (a well-known poison for metals arising from the precursor and evidenced by XPS analyses). As mentioned above, those chloride species were not observed in pre-reduced systems as they were eliminated as HCl during hydrogen pretreatment.

In order to cast further light on the effect of Ni oxidation states and the presence of chloride species on catalytic performance, some reutilisation studies were carried out on the Ni-0.5-DP catalyst both under UV and solar irradiation. Therefore, after 6 h irradiation, the solid was recovered by filtration, washed with methanol and acetone and dried at 110 °C. The catalyst was labelled as Ni-0.5-DP 1 using UV and Ni-0.5-DP 1 using solar, depending on the irradiation source. The solids were tested in another reaction, and the catalytic results are shown in Figure 10. As can be seen, hydrogen production dropped from 503 to 212 micromole per gram of catalyst after 6 h of UV irradiation, whereas no significant deactivation was observed under visible light. In any case, catalytic results were far below those achieved with fresh, pre-reduced catalysts.
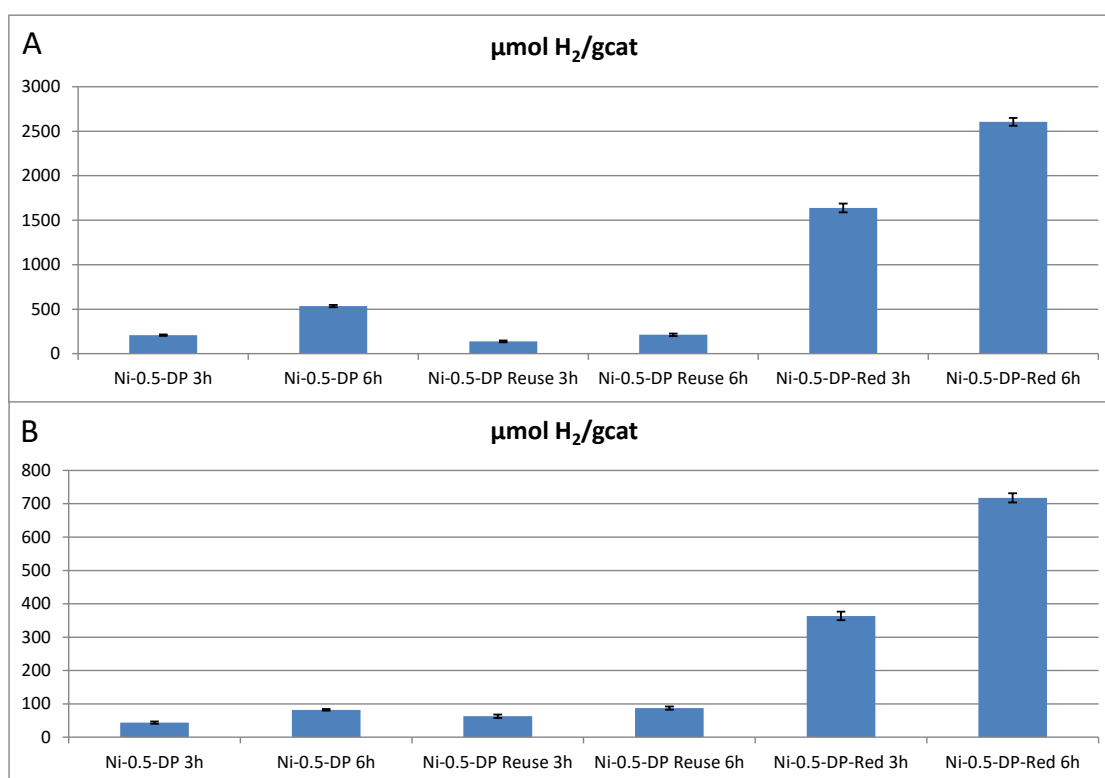
Figure 10. Comparison of hydrogen photocatalytic production on untreated Ni-0.5-DP after the first and second use using UV light (**A**) or solar light (**B**). For the sake of comparison, results obtained for the pre-reduced solid (Ni-0.5-DP-Red) have also been included.

TEM micrographs (Figure 5) did not evidence any significant increase in Ni particle size with the first use. After the second use, the metal particle size only slightly increased for solar irradiation studies.

XPS experiments (Table 3) showed that surface chlorides had already been eliminated after the first use, and it is assumed that there had been an in-situ reduction of nickel species. Thus, neither the presence of chlorides nor the in-situ reduction of NiO can account for the possitive effect of pre-reduction treatment at 400 °C on catalytic performance. It is possible that such a pre-treatment induced a strong metal–support interaction (SMSI) [32,33] which somehow favored the subsequent catalytic performance. This SMSI would be favored on homogeneously-distributed particles achieved by the deposition–precipitation method, which could explain the above-mentioned better catalytic performance of Ni-0.5-DP-Red as compared to Ni-0.5-IMP-Red. Nevertheless, these hypothetical Ni–support interactions were not detected by XPS measurements and therefore require further studies.

4. Conclusions

Hydrogen production through the glycerol photo-reforming of titania-based systems was significantly improved on the incorporation of nickel (0.5% by weight) through deposition–precipitation (DP) or impregnation (IMP) methods. This improvement was more pronounced when solar light was used as the irradiation source. The absorption shift to the visible range in the presence of Ni (evidenced by UV-Vis) could account for this effect. The pre-reduction of the systems prior to the catalytic essays led to a substantial improvement in catalytic performance, despite the fact that XPS studies showed that i) nickel species were "in-situ" reduced under working conditions, and ii) surface chloride species (arising from the used precursor, $NiCl_2$) are removed as the reaction proceeds. It is possible that pre-reduction treatment at 400 °C induced a strong metal–support interaction (SMSI) which could be positive to the catalytic performance, although this requires further studies. This SMSI effect would be favored for systems with smaller, more uniformly-distributed Ni particle sizes synthesized by the DP

method as compared to the IMP method. This would be consistent with the observed higher activities of Ni-0.5-DP Red as compared to Ni-0.5-IMP Red. In summary, the addition of a small percentage (0.5% by weight) of a transition metal such as Ni (ca. 2000 times cheaper than Pt) resulted in a 15.5-fold increase in the catalytic activity of Evonik P25, producing 2.6 mmol $H_2 \cdot g^{-1}$ after 6 h of UV irradiation. Thus, Ni proved to be a promising metal for use in photo-reforming processes of biomass-derived oxygenated compounds.

Supplementary Materials: The following are available online at http://www.mdpi.com/1996-1073/12/17/3351/s1. Figure S1. Hydrogen calibration plot used in this work. Figure S2. A typical chromatogram obtained in the hydrogen quantification process through GC. Figure S3. X-ray diffractograms of Evonik P25, Ni-0.5-DP. Ni-0.5-IMP, Ni-0.5-DP-Red and Ni-0.5-IMP-Red. Figure S4. Band-gap energy (Eg) calculation for the Ni-0.5-IMP-Red catalysts. Figure S5. Particle size distribution of each catalyst. Figure S6. XPS profiles for the Ni 2p3/2 component of each catalyst.

Author Contributions: Conceptualization, A.M. and F.J.U.; methodology, J.H-C. and A.M.; validation, F.J.U., A.M. and J.H.-C.; formal analysis, A.M. and J.H-C; investigation, J.M-G., J.M. and J.C.E.; data curation, A.M., J.H.-C.; writing—original draft preparation, J.M.-G. and J.H.C.; writing—review and editing, F.J.U. and A.M.; supervision, J.H-C., F.J.U. and A.M.

Conflicts of Interest: The authors declare no conflict of interest.

References

1. Melián, E.P.; López, C.R.; Santiago, D.E.; Quesada-Cabrera, R.; Méndez, J.A.O.; Rodríguez, J.M.D.; Díaz, O.G. Study of the photocatalytic activity of Pt-modified commercial TiO$_2$ for hydrogen production in the presence of common organic sacrificial agents. *Appl. Catal. A Gen.* **2016**, *518*, 189–197. [CrossRef]

2. Granada Ramírez, O.; Gutierrez Arzaluz, M.; Ávila Jiménez, M.; Fernández Sánchez, L.; Aguilar Pliego, J.; Mugica Álvarez, V.; Torres Rodríguez, M. Oxidación de glicerol en fase acuosa con platino soportado en óxido de titanio. *Superf. Vacío* **2016**, *29*, 9–13.

3. Avgouropoulos, G.; Ioannides, T.; Kallitsis, J.K.; Neophytides, S. Development of an internal reforming alcohol fuel cell: Concept, challenges and opportunities. *Chem. Eng. J.* **2011**, *176*, 95–101. [CrossRef]

4. Du, C.; Mo, J.; Li, H. Renewable Hydrogen Production by Alcohols Reforming Using Plasma and Plasma-Catalytic Technologies: Challenges and Opportunities. *Chem. Rev.* **2015**, *115*, 1503–1542. [CrossRef] [PubMed]

5. Singh, R.; White, D.; Demirel, Y.; Kelly, R.; Noll, K.; Blum, P. Uncoupling Fermentative Synthesis of Molecular Hydrogen from Biomass Formation in Thermotoga maritima. *Appl. Environ. Microbiol.* **2018**, *84*, e00998-18. [CrossRef] [PubMed]

6. Singh, R.; Tevatia, R.; White, D.; Demirel, Y.; Blum, P. Comparative kinetic modeling of growth and molecular hydrogen overproduction by engineered strains of Thermotoga maritima. *Int. J. Hydrogen Energy* **2019**, *44*, 7125–7136. [CrossRef]

7. Bednarczyk, K.; Stelmachowski, M.; Gmurek, M. The Influence of Process Parameters on Photocatalytic Hydrogen Production. *Environ. Prog. Sustain. Energy* **2018**, *38*, 680–687. [CrossRef]

8. Christoforidis, K.C.; Fornasiero, P. Photocatalytic Hydrogen Production: A Rift into the Future Energy Supply. *ChemCatChem* **2017**, *9*, 1523–1544. [CrossRef]

9. Wang, C.; Cai, X.; Chen, Y.; Cheng, Z.; Luo, X.; Mo, S.; Jia, L.; Lin, P.; Yang, Z. Improved hydrogen production from glycerol photoreforming over sol-gel derived TiO$_2$ coupled with metal oxides. *Chem. Eng. J.* **2017**, *317*, 522–532. [CrossRef]

10. Martínez, F.M.; Albiter, E.; Alfaro, S.; Luna, A.L.; Colbeau-Justin, C.; Barrera-Andrade, J.M.; Remita, H.; Valenzuela, M.A. Hydrogen Production from Glycerol Photoreforming on TiO$_2$/HKUST-1 Composites: Effect of Preparation Method. *Catalysts* **2019**, *9*, 338. [CrossRef]

11. Barreca, D.; Carraro, G.; Gombac, V.; Gasparotto, A.; Maccato, C.; Fornasiero, P.; Tondello, E. Supported metal oxide nanosystems for hydrogen photogeneration: Quo vadis? *Adv. Funct. Mater.* **2011**, *21*, 2611–2623. [CrossRef]

12. Chen, X.; Selloni, A. Introduction: Titanium Dioxide (TiO$_2$) Nanomaterials. *Chem. Rev.* **2014**, *114*, 9281–9282. [CrossRef] [PubMed]

13. Kumaravel, V.; Mathew, S.; Bartlett, J.; Pillai, S.C. Photocatalytic hydrogen production using metal doped TiO$_2$: A review of recent advances. *Appl. Catal. B Environ.* **2019**, *244*, 1021–1064. [CrossRef]

14. Daghrir, R.; Drogui, P.; Robert, D. Modified TiO$_2$ For Environmental Photocatalytic Applications: A Review. *Ind. Eng. Chem. Res.* **2013**, *52*, 3581–3599. [CrossRef]

15. Zhang, J.; Huang, Y.; Dan, Y.; Jiang, L. P3HT/Ag/TiO$_2$ ternary photocatalyst with significantly enhanced activity under both visible light and ultraviolet irradiation. *Appl. Surf. Sci.* **2019**, *488*, 228–236. [CrossRef]

16. Jovic, V.; Chen, W.-T.; Sun-Waterhouse, D.; Blackford, M.G.; Idriss, H.; Waterhouse, G.I.N. Effect of gold loading and TiO$_2$ support composition on the activity of Au/TiO$_2$ photocatalysts for H$_2$ production from ethanol–water mixtures. *J. Catal.* **2013**, *305*, 307–317. [CrossRef]

17. López-Tenllado, F.J.; Hidalgo-Carrillo, J.; Montes, V.; Marinas, A.; Urbano, F.J.; Marinas, J.M.; Ilieva, L.; Tabakova, T.; Reid, F. A comparative study of hydrogen photocatalytic production from glycerol and propan-2-ol on M/TiO$_2$ systems (M = Au, Pt, Pd). *Catal. Today* **2017**, *280*, 58–64. [CrossRef]

18. Bowker, M.; Morton, C.; Kennedy, J.; Bahruji, H.; Greves, J.; Jones, W.; Davies, P.R.; Brookes, C.; Wells, P.P.; Dimitratos, N. Hydrogen production by photoreforming of biofuels using Au, Pd and Au–Pd/TiO$_2$ photocatalysts. *J. Catal.* **2014**, *310*, 10–15. [CrossRef]

19. Carraro, G.; MacCato, C.; Gasparotto, A.; Montini, T.; Turner, S.; Lebedev, O.I.; Gombac, V.; Adami, G.; Van Tendeloo, G.; Barreca, D.; et al. Enhanced hydrogen production by photoreforming of renewable oxygenates through nanostructured Fe$_2$O$_3$ polymorphs. *Adv. Funct. Mater.* **2014**, *24*, 372–378. [CrossRef]

20. Iriondo, A.; Barrio, V.L.; Cambra, J.F.; Arias, P.L.; Guemez, M.B.; Sanchez-Sanchez, M.C.; Navarro, R.M.; Fierro, J.L.G. Glycerol steam reforming over Ni catalysts supported on ceria and ceria-promoted alumina. *Int. J. Hydrogen Energy* **2010**, *35*, 11622–11633. [CrossRef]

21. Chen, W.-T.; Chan, A.; Sun-Waterhouse, D.; Llorca, J.; Idriss, H.; Waterhouse, G.I.N. Performance comparison of Ni/TiO$_2$ and Au/TiO$_2$ photocatalysts for H$_2$ production in different alcohol-water mixtures. *J. Catal.* **2018**, *367*, 27–42. [CrossRef]

22. Clarizia, L.; Vitiello, G.; Pallotti, D.K.; Silvestri, B.; Nadagouda, M.; Lettieri, S.; Luciani, G.; Andreozzi, R.; Maddalena, P.; Marotta, R. Effect of surface properties of copper-modified commercial titanium dioxide photocatalysts on hydrogen production through photoreforming of alcohols. *Int. J. Hydrogen Energy* **2017**, *42*, 28349–28362. [CrossRef]

23. Luciani, G.; Vitiello, G.; Clarizia, L.; Abdelraheem, W.; Esposito, S.; Bonelli, B.; Ditaranto, N.; Vergara, A.; Nadagouda, M.; Dionysiou, D.D.; et al. Near UV-irradiation of CuOx-impregnated TiO$_2$ providing active species for H$_2$ production through methanol photoreforming. *ChemCatChem* **2019**, *45324*, 1–14.

24. Li, C.; Chen, Y.W. Temperature-programmed-reduction studies of nickel oxide/alumina catalysts: Effects of the preparation method. *Thermochim. Acta* **1995**, *256*, 457–465. [CrossRef]

25. Petrik, I.S.; Krylova, G.V.; Lutsenko, L.V.; Smirnova, N.P.; Oleksenko, L.P. XPS and TPR study of sol-gel derived M/TiO$_2$ powders (M = Co, Cu, Mn, Ni). *Chem. Phys. Technol. Surf.* **2015**, *6*, 179–189.

26. Carley, A.F.; Jackson, S.D.; O'Shea, J.N.; Roberts, M.W. The formation and characterisation of Ni3+—An X-ray photoelectron spectroscopic investigation of potassium-doped Ni(1 1 0)-O. *Surf. Sci.* **1999**, *440*, L868–L874. [CrossRef]

27. Janlamool, J.; Jongsomjit, B. Characteristics and catalytic properties of Ni/Ti-Si composite oxide catalysts via CO$_2$ hydrogenation. *Eng. J.* **2017**, *21*, 45–55.

28. Ju, F.; Wang, M.; Wu, T.; Ling, H. The role of NiO in reactive adsorption desulfurization over NiO/ZnO-Al$_2$O$_3$-SiO$_2$ adsorbent. *Catalysts* **2019**, *9*, 79. [CrossRef]

29. Morales, J. Hydrogen Production by Glycerol Photo-Reforming, Using Noble and Transition Metals Supported on Titanium Dioxide. Master's Thesis, University of Córdoba (SPAIN), Cordoba, Spain, 2018.

30. Bahruji, H.; Bowker, M.; Davies, P.R.; Kennedy, J.; Morgan, D.J. The importance of metal reducibility for the photo-reforming of methanol on transition metal-TiO$_2$ photocatalysts and the use of non-precious metals. *Int. J. Hydrogen Energy* **2015**, *40*, 1465–1471. [CrossRef]

31. Caravaca, A.; Jones, W.; Hardacre, C.; Bowker, M. H$_2$ production by the photocatalytic reforming of cellulose and raw biomass using Ni, Pd, Pt and Au on titania. *Proc. R. Soc. A Math. Phys. Eng. Sci.* **2016**, *472*, 20160054. [CrossRef]

32. Colmenares, J.C.; Magdziarz, A.; Aramendia, M.A.; Marinas, A.; Marinas, J.M.; Urbano, F.J.; Navio, J.A. Influence of the strong metal support interaction effect (SMSI) of Pt/TiO$_2$ and Pd/TiO$_2$ systems in the photocatalytic biohydrogen production from glucose solution. *Catal. Commun.* **2011**, *16*, 1–6. [CrossRef]

33. Szabó, F.Z.G. *Solymosi in "Proceedings, 2nd International Congress on Catalysis"*; Technip: Paris, France, 1961; p. 1627.